NANO LETTERS

2008
Vol. 8, No. 8
2345-2350

Mapping the Polarization Pattern of Plasmon Modes Reveals Nanoparticle Symmetry

Olaf Schubert, Jan Becker, Luigi Carbone, Yuriy Khalavka, Tetyana Provalska, Inga Zins, and Carsten Sönnichsen*

Institute of Physical Chemistry, University of Mainz, Jakob-Welder-Weg 11, 55128 Mainz, Germany

Received April 25, 2008; Revised Manuscript Received June 4, 2008

ABSTRACT

We study the wavelength and polarization dependent plasmon resonances of single silver and gold nanorods, triangles, cubes, and dimers with a novel single particle spectroscopy method (RotPOL). In RotPOL, a rotating wedge-shaped polarizer encodes the full polarization information of each particle within one image. This reveals the symmetry of the particles and their plasmon modes, allows analyzing inhomogeneous samples and the monitoring of particle shape changes during growth in situ.

Plasmon resonances of noble metal nanoparticles are explored for single molecule labeling, cancer-treatment, enhancement of nonlinear optical effects, or light guiding.[1,2] Often, the degree and direction of polarization of the scattered light is essential.[3] Polarization analysis of light from single fluorescent emitters has been a major advancement in single molecule optics used to study the conformational dynamics of biomolecules and their spatial arrangement.[4] There are several techniques (among them polarization modulation,[5] defocusing,[6,7] back-plane imaging,[8] or polarization analysis[9]), which give the orientation of an emission or absorption dipole but not the degree and symmetry of the emitted light polarization itself. For the dipolar emission of typical fluorescent molecules, the $\cos^2 \theta$ dependency of the light intensity on the polarization angle θ is well known and usually not at the center of interest. For light emission of larger nanoparticles, the light emission is not necessarily of dipolar character.[10] In particular, the resonant light scattering from plasmons in noble metal particles is expected to show the symmetry of the oscillation mode and the particle shape. At different wavelengths of the excitation light, different oscillation modes are excited making it important to know the polarization pattern as a function of wavelength. Knowing the polarization pattern of plasmonic nanostructures is therefore not only important to understand the fundamental physics of light interaction with these structures, but allows one to discriminate different oscillation modes within one particle and to distinguish differently shaped particles within one sample. Several techniques have been used to extract optical spectra of single plasmonic nanoparticles,[11–14] most efficiently using dark-field microscopy, but little is known about the polarization state. So far, the very few reported plasmon polarization studies were obtained by rotating a polarizer by hand[15,16] or on ensembles[17] and not combined with spectroscopic information.

Our rotPOL approach uses a wedge-shaped quickly rotating polarizer (rotPL, Figure 1a), which splits the light of a point source into a ring in the image plane encoding the polarization information in a spatial image (Figure 1b). The polarization intensity in a given direction is simply taken from the corresponding position on this ring recorded with an exposure time large compared to the rotation time (Figure 1c). A dipole, for example, will show two loops at opposite sides (Figure 1a). We combine this rotating polarizer with a standard transmission dark-field microscope with white light excitation from a 100 W halogen lamp, 40× water-immersion objective (NA 0.8) and a high numerical aperture condenser (NA 1.2−1.4). To simultaneously record spectral and polarization information (Figure 1d) we place a variable wavelength interference filter (varIF, *VERIL S 200*, Schott AG) in front of the digital camera (either a peltier-cooled CCD (CoolSnapHQ2, Photometrics) or a consumer digital DSL camera (EOS 400D, Canon)). The filter transmits light only in a narrow wavelength window and, in combination with a stepper motor (T-LLS260, Zaber Technologies Inc.), serves as a convenient and inexpensive imaging spectrometer.

The combination (rotPL, varIF) allows the recording of single particle scattering spectra $I(\lambda)$, the polarization anisotropy PA(λ), and/or the determination of full wavelength

* To whom correspondence should be addressed. E-mail: Soennichsen@uni-mainz.de.

10.1021/nl801179a CCC: $40.75
Published on Web 07/01/2008

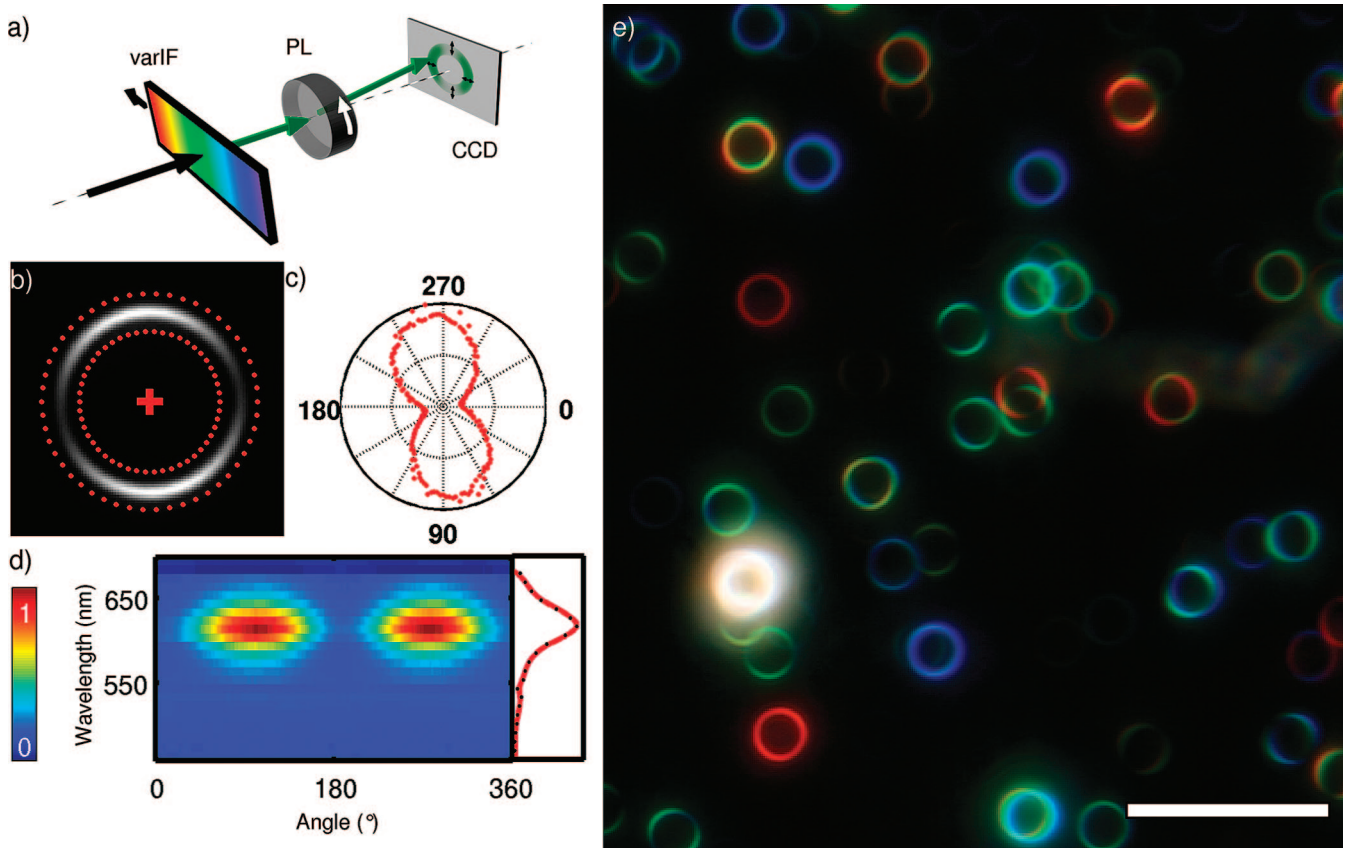

Figure 1. (a) Schematics of the rotPOL setup. One wavelength is selected by a linear variable interference filter (varIF), then the light is dispersed into the different polarization directions by a wedge-shaped rotating polarizer (PL), resulting in ring-shaped intensity profiles of a pointlike light source on the digital camera (b). In order to get the polarization profile shown in (c) (intensity $I(\theta)$) as a function of polarization angle θ), we integrate the image between an inner and outer ring diameter (dashed lines in panel b). The center of the rings is chosen to minimize asymmetry between opposite sides. Repeating this procedure for each wavelength produces intensity values as a function of wavelength and polarization angle $I(\lambda, \theta)$, which we show color-coded in (d). The same analysis is possible for all particles within the field of view in parallel. (e) Real-color image of an inhomogeneous silver sample containing spheres, rods, and triangles as seen through the rotPol-microscope. Two colors in one ring correspond to two different plasmon modes at the respective wavelengths. Scalebar is 25 μm.

and polarization dependent scattering intensity $I(\theta,\lambda)$ for up to 50 particles in parallel. The polarization anisotropy $PA(\lambda)$ is defined as[18] $PA(\lambda) = (I_a - I_b)/(I_a + I_b)$, where I_a and I_b correspond to the scattering intensity of light polarized parallel to the major and minor particle axis, respectively. For rodlike particles, $PA(\lambda)$ may become negative near the short axis resonance, where I_b is high. We tested the polarization inhomogeneity of the setup itself, by measuring polarization-dependent spectra of perfectly spherical SiO2-spheres (∅ 314 nm, Corpuscular Inc.) and obtained a median PA of 0.1 (see Supporting Information, Figure S10). The error in the polarization values obtained in this work is therefore about 0.1.

To compare our experimental results to theory, we simulated polarization dependent spectra of rod-shaped, cubic, and triangular gold and silver particles within the discrete dipole approximation (DDA, see Supporting Information, Figure S8) using the particle sizes and shapes determined by transmission electron microscopy (TEM). Particle sizes and shapes vary significantly within one batch of nanoparticles. Since we are not able to measure identical particles with rotPOL and TEM, the simulations have some degree of freedom regarding the precise particle dimensions.

To explore the possible polarization states of simple plasmonic nanostructures, we determine the wavelength and polarization dependent scattering intensity $I(\theta, \lambda)$ of gold and silver rods, triangles, spheres, and pairs of spheres (representative examples in Figure 2, synthesis procedures,[19–23] more particles and further details about the setup in the Supporting Information, Figures S1, S2, S3, S4, and S5).

The qualitative results for all investigated nanoparticles agree well with simulations (Figure 2). Interesting is the complete absence of polarization anisotropy for silver cubes both in theory and experiment, which surprised us at first. However, two orthogonal dipoles with $\cos^2\theta$ intensity dependency cancel each other out completely ($\cos^2\theta + \sin^2\theta = 1$). Rods show the expected dipolar behavior with sometimes the short axis peak visible at lower wavelength in the orthogonal direction. In samples containing only spheres, some particles show an unexpectedly high PA combined with a red-shifted resonance wavelength. The polarization dependent spectra of these particles agree well with simulations of a pair of

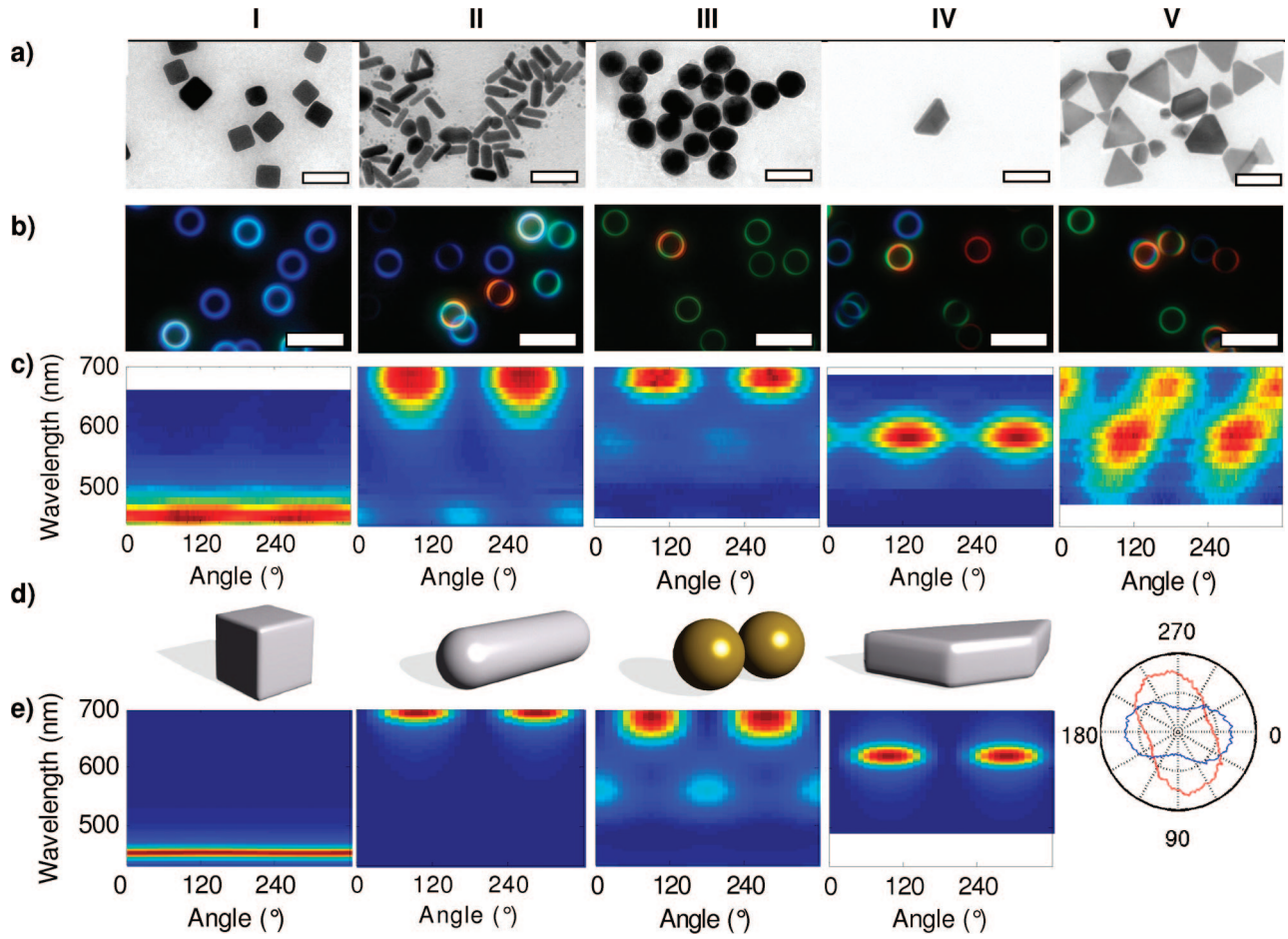

Figure 2. Typical plasmon polarization results for simple gold and silver plasmonic nanostructures. (a) TEM images of samples containing silver (I,II,IV,V) and gold (III) nanoparticles (scale bar: 100 nm). In line (b), typical real-color microscopic images of those samples are shown (scale bar: 15 μm). The polarization dependent single-particle-scattering-spectra $I(\lambda, \theta)$ of representative particles are shown in (c) color-coded as in Figure 1. These results can be compared to simulations by discrete dipole approximation shown in (e) with the model sketched in (d) For the triangular particle in column V, a polar graph of the intensity $I(\theta)$ at the two particle resonances visible in Vc is shown in the bottom panel. Two loops with the expected 60° offset are clearly visible.

two spheres within close distance. The shift of the plasmon mode along the interparticle axis ("long axis") depends strongly on the interparticle distance.[24] Measuring $I(\lambda, \theta)$ allows the extraction of the orientation of the particle pair, the interparticle spacing ("plasmon ruler")[25] and may allow the construction of a "self-calibrating" plasmonic ruler insensitive to changes in the dielectric environment. Samples containing triangles show very often "rodlike" resonances, which is probably due to a shape asymmetry of the triangles. The DDA simulations of such "truncated triangles" show reasonable agreement with measured spectra. Since it is not easily possible to correlate directly particle shape and optical spectra and our samples of triangles are particularly polydisperse, the interpretation remains tentative. In some polarization spectra $I(\lambda, \theta)$, we observe the 60° symmetry expected for triangles. In the cases where we observed this 60° symmetry, each resonance was shifted in wavelength (Figure 2, particle V), again most likely due to small differences for the plasmon modes in the direction of the three corners. We were not able to simulate the polarization spectrum $I(\lambda, \theta)$ of such particles so far due to the high number of possible ways to modify the corners.

Nanorods are the most often used and conceptually most simple "antenna-like" plasmonic structures, and it is therefore important to study their emission pattern more closely. We measure polarization dependent single particle scattering spectra $I(\theta, \lambda)$ for rod-shaped gold nanoparticles (average sizes 57 × 28 nm) and compare those with two batches of spherical gold particles with nominal diameters of 60 and 80 nm, respectively (Figure 3). First, we extract the polarization anisotropy PA at the resonance wavelength λ_{res}. As expected, rod-shaped particles show a high degree of polarization anisotropy (average PA(λ_{res}) 0.84, Figure 3a)[15] while spherical particles had an average PA(λ_{res}) of about 0.35 (Figure 3a). Looking at the polarization anisotropy PA(λ) over the full optical spectrum, we observe almost no wavelength dependency for spheres, but a strong spectral dependency for rods. This reflects the lack of excitation of the long-axis plasmon mode with light-waves out-of-resonance. We found it surprising at first that the spheres showed a PA(λ_{res}) much greater than zero. We found for the nominally round particles a mean aspect ratio (shape anisotropy) from TEM images of about 1.1. (see Supporting Information, Figure S11).

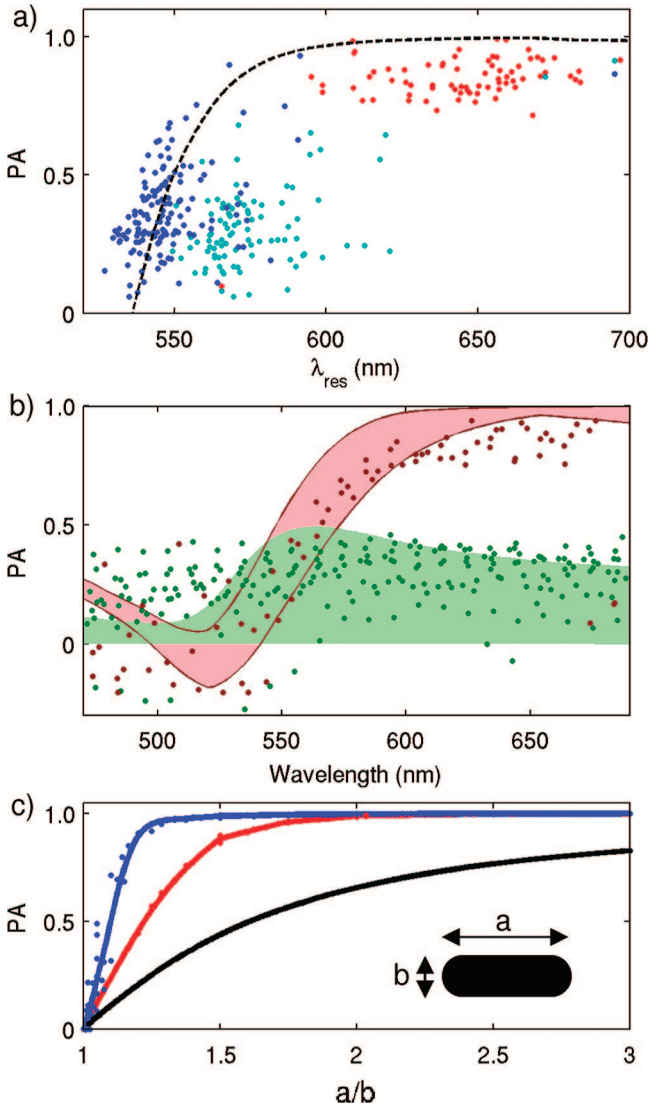

Figure 3. (a) The polarization anisotropy $PA(\lambda_{res}) = (I_a - I_b)/(I_a + I_b)$ at the longitudinal plasmon resonance wavelength λ_{res} is shown as a function of the resonance wavelength for three different gold particle samples (blue dots, nominally spherical gold particles with 60 nm diameter; 87 nm diameter, teal dots; and red dots, gold nanorods). We extract each point from a full wavelength and polarization dependent single particle scattering spectrum $I(\theta, \lambda)$. The dashed black line is a theoretical prediction from simulations of gold rods of different aspect ratios and sizes embedded in water (refractive index $n = 1.34$). The polarization anisotropy $PA(\lambda)$ for a given particle varies as a function of wavelength λ, which we show in (b) for gold rods (red dots) and spheres (green dots). The shaded red and green areas correspond to theoretical predictions for particles with aspect ratios (a/b) of $2 < a/b < 3$ and $a/b < 1.2$, respectively. The theoretical prediction of polarization anisotropy PA at the resonance wavelength as a function of aspect ratio (a/b) for silver (blue dots), gold (red dots) and SiO2 (black dots) particles is shown in (c). Dots correspond to DDA-simulations, the lines are fits. The simulations do not perfectly follow a common trend due to a small influence of particle volume on the polarization anisotropy.

Simulations for Ag, Au, and SiO_2-particles (Figure 3c) show that the strong sensitivity of the polarization anisotropy is a plasmonic effect: gold and silver particles with an aspect ratio as low as 1.8 and 1.6 (respectively) already have a PA of 0.9, for SiO_2 this value is reached only for an aspect ratio

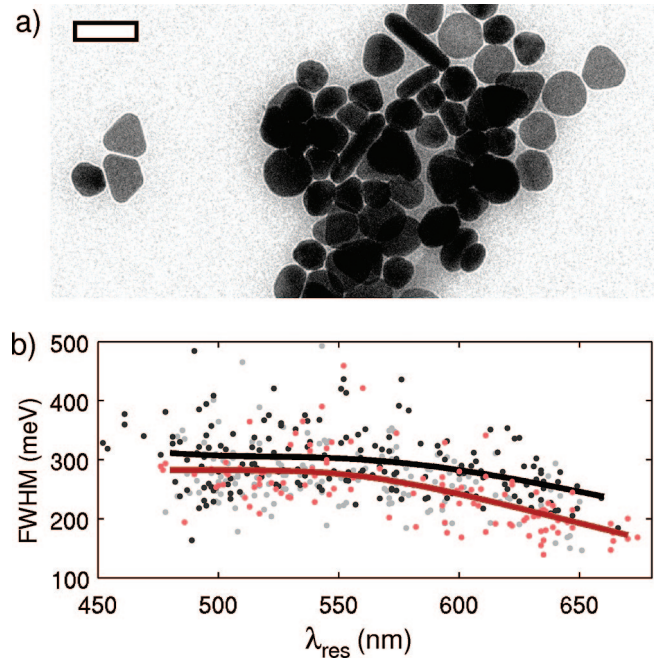

Figure 4. Polarization analysis of an inhomogeneous silver sample. In a typical TEM image of an inhomogeneous silver sample (a), rods, spheres, and triangles are present. We measure the plasmon line width (full width at half-maximum, fwhm) of individual particles as a function of their resonance energy wavelength (λ_{res}) for different silver samples (b). Each dot corresponds to one particle, for which the full wavelength and polarization dependent scattering intensity $I(\lambda, \theta)$ was determined (see Supporting Information, Figure S12) and the polarization anisotropy at the resonance wavelength $PA(\lambda_{res})$ extracted. On average, particles with a high PA (PA > 0.7, red dots) show a lower line width than particles with a low PA (<0.5, black dots). The lines represent the average line width for the two subpopulations.

of 4. The plasmon damping in silver is lower than in gold, which may explain the steeper $PA(a/b)$ function. These theoretical results explain the unexpectedly high polarization anisotropy of nominally round gold spheres.

Another possible advantage of obtaining polarization dependent scattering spectra $I(\lambda, \theta)$ of single plasmonic nanostructures is the analysis of subpopulations in very inhomogeneous samples. For example, silver nanoparticle preparations often contain a mixture of triangles, rods, and spheres (Figure 4a) and their separation is tedious.[26] For such inhomogeneous silver samples, we determined $I(\lambda, \theta)$ for 754 particles. We find that the line width of the main resonance is in general lower for particles with a high $PA(\lambda_{res})$, compared to particles with a low $PA(\lambda_{res})$ (Figure 4b). If we identify particles with a high $PA(\lambda_{res})$ with rods, the experimental results can be interpreted as a lower plasmon damping in rods compared to spherical or platelike particles, even when comparing particles at the same resonance wavelength. The observed differences in plasmon damping at the same resonance wavelength are therefore a strong evidence for a shape or surface quality related plasmon damping mechanism.[27]

The rotPol method is not limited to static measurements but may record polarization dependent particle spectra with high temporal resolution, especially if spectral information

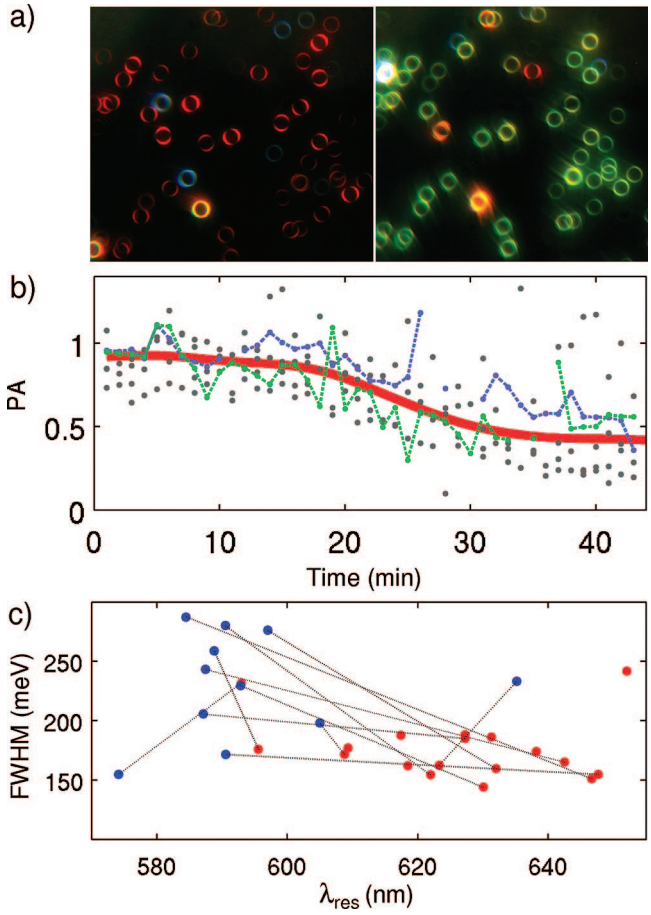

Figure 5. In situ particle growth observation of gold nanorods exposed to a growth solution. We record polarization information at the three RGB colors as a function of time using a consumer digital DSL camera. Starting with rod-shaped nanoparticles with high degree of polarization anisotropy and light scattering mostly in the red (a, left), the resonance wavelength decreases over time until the particles scatter light mostly in the green (a, right). The polarization anisotropy PA decreases over time until nearly all particles show a much lower anisotropy (b). Two typical trajectories of the PA for single particles are indicated as dashed lines in blue and green, the red line is an average over six particles. A video of the whole growth process is available in the Supporting Information, supplementary video 1. Before and after the growth process, detailed polarization-dependent scattering spectra $I(\lambda, \theta)$ are obtained. The line width fwhm and resonance wavelength λ_{res} extracted from these measurements are shown in (c) (red dots at start of growth process, blue dots afterward). Dashed lines connect dots corresponding to the same particle. For most particles, the resonance wavelength decreases and the line width increases. The decrease of polarization anisotropy over time, the simultaneous decrease in resonance wavelength, and the increase in line width suggest that the rod-shaped particles grow mainly along the short axis, resulting in particles that are more spherical.

is not required. We monitored the growth of 18 gold nanorods immobilized in a glass flow cell and exposed to a growth solution containing gold ions with a time resolution of 60 s using a consumer digital camera bypassing the interference filter (Figure 5a,b, video; see Supporting Information, Figure S5). We observe a decrease of the average polarization anisotropy (PA) over time from 0.9 to 0.4 within 43 min. This decrease of PA is consistent with the decrease of aspect ratio for gold rods exposed to a growth solution due to the preferential growth in width we observed before.[28] To confirm the preferential growth in width, full polarization dependent scattering spectra $I(\theta, \lambda)$ were recorded before and after the growth-process for a subset of 16 particles. A shift of the resonance wavelength to lower wavelengths and an increase in line width is observed for most particles as expected for larger, rounder nanoparticles.

The rotPOL method is therefore a versatile tool to study polarization anisotropy of the light emission pattern from nanoparticles, especially for plasmonic structures but possibly also for fluorescent quantum structures. The large variety of plasmon emission patterns observed for the simple particle morphologies investigated here (spheres, rods, triangles, cubes, and particle pairs) provide a wide field for optimization for applications such as light guiding and allow detailed theoretical modeling of plasmon modes. The high polarization anisotropy found for even moderately elongated spheres highlights the strong influence of polarization even for nominally round particles. The possibility to record dynamic changes of the polarization emission pattern of single particles allows studying particle growths modes *in situ* and improving schemes for single nanoparticle binding and distancing assays.

Acknowledgment. We thank Georg Conrad, Nicolas Katte, and Markus Tacke for help and support and B. Draine and P. Flatau for making their DDA-code DDScat publicly available. Financial support was provided by the German Science Foundation (DFG) through an Emmy-Noether Research Grant and by the European Union through the NanoSciERA program. J.B. was supported by the Carl Zeiss foundation and Y.K by MATCOR. T.P. acknowledges helpful discussions with Oleksandra Korovyanko.

Supporting Information Available: Detailed experimental methods, real color images as obtained using RotPOL for different samples (Figures S1−S4), details of the growth process (Figures S05 and S06, Video SV-1), shapes used for DDA simulations (Figure S8), stability and reliability of the setup (Figures S9 and S10), TEM images and shape-histograms for gold spheres, and polarization dependent single particle spectra (Figure S12). This material is available free of charge via the Internet at http://pubs.acs.org.

References

(1) Murphy, C. J.; Gole, A. M.; Hunyadi, S. E.; Stone, J. W.; Sisco, P. N.; Alkilany, A.; Kinard, B. E.; Hankins, P. *Chem. Commun.* **2008**, 544–557.
(2) Maier, S. A.; Atwater, H. A. *J. Appl. Phys.* **2005**, *98*, 011101.
(3) Yang, H. *J. Phys. Chem. A* **2007**, *111*, 4987–4997.
(4) Weiss, S. *Nat. Struct. Biol.* **2000**, *7*, 724–729.
(5) Ha, T.; Laurence, T. A.; Chemla, D. S.; Weiss, S. *J. Phys. Chem. B* **1999**, *103*, 6839–6850.
(6) Bartko, A. P.; Dickson, R. M. *J. Phys. Chem. B* **1999**, *103*, 11237–11241.
(7) Toprak, E.; Enderlein, J.; Syed, S.; McKinney, S. A.; Petschek, R. G.; Ha, T.; Goldman, Y. E.; Selvin, P. R. *Proc. Natl. Acad. Sci. U.S.A.* **2006**, *103*, 6495–6499.
(8) Lieb, M. A.; Zavislan, J. M.; Novotny, L. *J. Opt. Soc. Am. B* **2004**, *21*, 1210–1215.
(9) Chung, I. H.; Shimizu, K. T.; Bawendi, M. G. *Proc. Natl. Acad. Sci. U.S.A.* **2003**, *100*, 405–408.

(10) Nelayah, J.; Kociak, M.; Stephan, O.; Garcia de Abajo, F. J.; Tence, M.; Henrard, L.; Taverna, D.; Pastoriza-Santos, I.; Liz-Marzan, L. M.; Colliex, C. *Nat. Phys.* **2007**, *3*, 348–353.
(11) Kalkbrenner, T.; Hakanson, U.; Sandoghdar, V. *Nano Lett.* **2004**, *4*, 2309–2314.
(12) Van Dijk, M. A.; Lippitz, M.; Orrit, M. *Acc. Chem. Res.* **2005**, *38*, 594–601.
(13) Arbouet, A.; Christofilos, D.; Del Fatti, N.; Vallee, F.; Huntzinger, J. R.; Arnaud, L.; Billaud, P.; Broyer, M. *Phys. Rev. Lett.* **2004**, *93*, 127401.
(14) Bosman, M.; Keast, V. J.; Watanabe, M.; Maaroof, A. I.; Cortie, M. B. *Nanotechnology* **2007**, *18*, 165505.
(15) Sönnichsen, C.; Franzl, T.; Wilk, T.; von Plessen, G.; Feldmann, J.; Wilson, O.; Mulvaney, P. *Phys. Rev. Lett.* **2002**, *88*, 077402.
(16) Müller, J.; Sönnichsen, C.; von Poschinger, H.; von Plessen, G.; Klar, T. A.; Feldmann, J. *Appl. Phys. Lett.* **2002**, *81*, 171–173.
(17) Perez-Juste, J.; Rodriguez-Gonzalez, B.; Mulvaney, P.; Liz-Marzan, L. M. *Adv. Funct. Mater.* **2005**, *15*, 1065–1071.
(18) Yguerabide, J.; Yguerabide, E. E. *Anal. Biochem.* **1998**, *262*, 137–156.
(19) Nikoobakht, B.; El-Sayed, M. A. *Chem. Mater.* **2003**, *15*, 1957–1962.
(20) Jana, N. R.; Gearheart, L.; Murphy, C. J. *Chem. Commun.* **2001**, 617–618.
(21) Sun, Y. A.; Xia, Y. N. *Adv. Mater.* **2003**, *15*, 695–699.
(22) Siekkinen, A. R.; McLellan, J. M.; Chen, J. Y.; Xia, Y. N. *Chem. Phys. Lett.* **2006**, *432*, 491–496.
(23) Draine, B. T.; Flatau, P. J. arXiv:astro-ph/0409262v22004.
(24) Reinhard, B. M.; Siu, M.; Agarwal, H.; Alivisatos, A. P.; Liphardt, J. *Nano Lett.* **2005**, *5*, 2246–2252.
(25) Sönnichsen, C.; Reinhard, B. M.; Liphardt, J.; Alivisatos, A. P. *Nat. Biotechnol.* **2005**, *23*, 741–745.
(26) Hanauer, M.; Pierrat, S.; Zins, I.; Lotz, A.; Sönnichsen, C. *Nano Lett.* **2007**, *7*, 2881–2885.
(27) Novo, C.; Gomez, D.; Perez-Juste, J.; Zhang, Z. Y.; Petrova, H.; Reismann, M.; Mulvaney, P.; Hartland, G. V. *Phys. Chem. Chem. Phys.* **2006**, *8*, 3540–3546.
(28) Becker, J.; Schubert, O.; Sönnichsen, C. *Nano Lett.* **2007**, *7*, 1664–1669.

NL801179A